

# Array Observations of the 2012 Haida Gwaii Tsunami Using Cascadia Initiative Absolute and Differential Seafloor Pressure Gauges

by Anne F. Sheehan, Aditya Riadi Gusman, Mohammad Heidarzadeh, and Kenji Satake

## INTRODUCTION

The purpose of this article is to test the ability of the seafloor pressure sensors utilized in the Cascadia Initiative (CI) experiment (Toomey *et al.*, 2014) to provide useful recordings of tsunamis, and to compare the performance of the different types of seafloor pressure sensors for long-period recordings. These tests are performed through analysis of CI seafloor pressure recordings of the 2012 Haida Gwaii tsunami.

Seafloor pressure measurements are a central part of tsunami warning systems. Deep-ocean Assessment and Reporting of Tsunamis (DART) buoy systems, designed by National Oceanic and Atmospheric Administration (NOAA), are equipped with seafloor pressure sensors (also referred to as bottom pressure recorders [BPRs]), providing tsunami data in real time (Eble and González, 1991; González *et al.*, 1998; Bernard *et al.*, 2001; Meinig *et al.*, 2005; Titov *et al.*, 2005; Mofjeld, 2009; Rabinovich and Eble, 2015). The DART instruments are widely spaced in deep water (typically > 2700 m) along coastal regions and near subduction zones. Cabled BPR arrays are becoming more common, such as the BPR array of NorthEast Pacific Time-Series Undersea Networked Experiments (NEPTUNE)-Canada ocean observatory (Thomson *et al.*, 2011), the Japan Agency for Marine-Earth Science and Technology (JAMSTEC) BPR array (Baba *et al.*, 2004; Saito *et al.*, 2010), and the BPR array in the Cascadia basin (Rabinovich *et al.*, 2011). Observations of tsunamis have also been made serendipitously on pressure gauges accompanying a variety of nontsunami field programs (e.g., Drushka *et al.*, 2008; Lin *et al.*, 2015).

In this study, we use seafloor pressure measurements from absolute pressure gauges (APGs), differential pressure gauges (DPGs), and DART BPRs to study the tsunami caused by the 2012 Haida Gwaii earthquake. The APG, used by the DART and increasingly in other oceanographic studies (Ito *et al.*, 2011; Chadwick *et al.*, 2012; Rawat *et al.*, 2014), makes use of a quartz transducer with oscillation period related to stress, and thus to pressure (Houston and Paros, 1998). The DPG is a pressure gauge configured to respond to the difference between the ocean pressure and the pressure within a confined volume of compressible oil (Cox *et al.*, 1984). It is often

installed with ocean-bottom seismometer (OBS) units as an alternative channel for the vertical seismic channel. *In situ* calibration of DPGs by comparison of Rayleigh waves recorded on the DPG to those from a collocated vertical-component OBS can be performed, but relies on a well-calibrated seismometer and is not necessarily valid outside the surface waveband (Takeo *et al.*, 2014). The use of tidal signals to calibrate DPGs has produced mixed results (Sheehan *et al.*, 2011), working best for deep-water stations, and may warrant further study. Tidal periods are longer than tsunami periods, and are farther outside the band that the DPGs were designed for. A previous study has estimated response of another style of DPG at long period by comparison with collocated APG (Araki and Sugioka, 2009). Recording of common signals on DPG, APG, and nearby DART stations provides us with an opportunity to compare the performance of these instruments and perform an *ad hoc* calibration in the tsunami frequency band.

## HAIDA GWAII EARTHQUAKE AND TSUNAMI

The 28 October 2012  $M_w$  7.8 Haida Gwaii earthquake (03:04:08 UTC, 52.788° N 132.101° W, depth 14.0 km,  $M_w$  7.8, United States Geological Survey, [http://earthquake.usgs.gov/earthquakes/eventpage/usp000juhz#scientific\\_origin](http://earthquake.usgs.gov/earthquakes/eventpage/usp000juhz#scientific_origin); last accessed July 2015) occurred off the west coast of Haida Gwaii (formerly the Queen Charlotte Islands), British Columbia. The earthquake involved westward-dipping thrust faulting along the transform boundary between the Pacific and North American plates (James *et al.*, 2015). Plate motions in the region are primarily taken up by strike-slip faulting parallel to the plate boundary, with lesser amounts of thrust faulting. The rupture propagated up-dip, with most slip occurring offshore, and involved seafloor uplift that generated a tsunami (Lay *et al.*, 2013). Local estimates of tsunami runup exceeding 3 m (maximum 13 m) were made from field surveys of deposits along the west coast of Haida Gwaii (Leonard and Bednarski, 2015). The tsunami was recorded by DART buoys and tide gauges throughout the northeast Pacific and Hawaii (Lay *et al.*, 2013; Fine *et al.*, 2014).

## SEAFLOOR PRESSURE DATA AND PROCESSING

The data for this study come from seafloor pressure gauges deployed as part of the CI (Tian *et al.*, 2013; Toomey *et al.*, 2014) and from NOAA DART stations (González *et al.*, 1998; Mungov *et al.*, 2013). The CI experiment is a 4-year experiment to study the offshore structure and seismic hazard of the Pacific northwest, through the use of deployment of 60+ OBS from 2011 to 2015. We use data from year 2 (2012–2013) of the CI in this study. The year 2 deployment consisted of coarse grids (~70 km spacing) throughout the Gorda plate and along the Cascadia subduction zone, a few stations on the Juan de Fuca and Pacific plates, and a dense concentration of OBSs at the Mendocino Triple Junction (Fig. 1). The OBSs were deployed in water depths from 60 to 4500 m, and the shallowest stations had protective shielding to deflect trawling nets.

The majority of the OBSs were provided by the United States National Ocean Bottom Seismograph Instrument Pool (OBSIP), which has three Institutional Instrument Contributors: Lamont Doherty Earth Observatory (LDEO), Scripps Institution of Oceanography (SIO), and Woods Hole Oceanographic Institution (WHOI). In addition to the OBSIP instruments 10 OBSs built with funding from the Keck Foundation were provided by WHOI. In addition to a broadband seismometer, each station was equipped with a seafloor pressure gauge (Table 1). Two different pressure gauge designs were utilized. The first is a Paroscientific APG (Houston and Paros, 1998; Polster *et al.*, 2009), which makes use of a quartz crystal resonator whose frequency of oscillation varies with pressure-induced stress (Meinig *et al.*, 2005; Polster *et al.*, 2009). The water temperature is also measured and a correction applied by the manufacturer (Rabinovich and Eble, 2015). All LDEO sites were equipped with an APG, as well as the DART stations. The second type of seafloor pressure gauge utilized is a Cox–Webb DPG (Cox *et al.*, 1984). The DPG sensor has three key parts: (1) a flexible rubber diaphragm, which admits the ocean pressure; (2) a reference chamber containing compressible oil; and (3) a strain gauge transducer, which responds to the difference of pressure between the ocean and the fluid in the reference chamber (Cox *et al.*, 1984; Webb *et al.*, 1991). It is found to be especially useful for detecting pressure fluctuations in the frequency range from a few millihertz to a few hertz but the rolloff toward the low frequency is gradual, which makes it possible to record tsunami signals. It can capture pressure fluctuation of several millimeters of water pressure, whereas DART bottom pressure recorders have a measurement sensitivity of < 1 mm at 6000 m water depth (Meinig *et al.*, 2005). Both the SIO and WHOI sites utilize DPGs. The WHOI DPG has an additional high-pass filter applied, and has individually calibrated sensors (values range by around 10%; instrument response parameters available from Incorporated Research Institutions for Seismology Data Management Center [IRIS DMC]).

Instrument response parameters for the APG and DPG instruments were obtained from the IRIS DMC and are shown in Figure 2. The APGs have flat instrument response to 0 Hz, making these instruments well suited for seafloor geodesy as well

as recording of tsunamis (typical tsunami period is approximately 1000 s). The DPGs have a corner period of 500 s for SIO and 30 s for WHOI instruments, which poses challenges in the tsunami passband, but the rolloff toward the low frequency is gradual, which makes it possible to record tsunami signals.

We retrieved CI APG and DPG waveforms from the IRIS DMC. Twelve-hour records were extracted, starting 3 hr before the Haida Gwaii earthquake origin time to 9 hr after the earthquake origin time, allowing more than enough time for both seismic and tsunami recordings at all stations. In cases where the waveforms were saturated (clipped) on the earthquake, the records were cut to begin after the clipped time. Clipping was on the large amplitude earthquake surface-wave arrivals, and tended to be on the stations closer to the source, but not necessarily. The stations ranged from 4.5° to 13° distance from the  $M_w$  7.8 Haida Gwaii earthquake. None of the LDEO APG instruments were clipped, 4 out of 15 SIO DPGs were clipped, and 12 out of 23 WHOI DPGs were clipped. Our data processing involved removing trend and mean from the data, decimation, band-pass filtering from 0.0002 to 0.005 Hz (5000–200 s), and removal of instrument response. The instrument response parameters, as supplied from the OBSIP to the IRIS DMC, were deconvolved from the pressure records, converting the data from instrument counts to pascals. The instrument response parameters consist of poles, zeros, and a constant (Table 2). The system frequency response is given by the ratio of two complex polynomials. The roots of the numerator polynomial are the instrument zeros, and the roots of the denominator polynomial are the instrument poles. We use the Seismic Analysis Code (SAC) transfer command to remove instrument type as defined by poles and zeros using spectral division. The deconvolution was accompanied by filtering, which was a particular issue with SIO DPGs that had long-period noise enhanced through the deconvolution. WHOI DPGs, even though corner frequency at 30 s, were stable to tsunami periods after deconvolution. Data were then converted from pascals to (variation in) sea surface height via the equation

$$b = P/(\rho g)$$

in which  $b$  is the sea surface height,  $P$  is seafloor pressure,  $\rho$  is density of seawater, and  $g$  is gravitational acceleration. DART data were obtained from the NOAA. DART data are already provided in units of wave height (meters) and instrument deconvolution is not required. The ocean tides were approximated by fitting a polynomial function to the original records and then removed from them.

## Tsunami SIMULATION

To simulate tsunami propagation, we numerically solved the linear shallow water equations using a finite-difference method (Satake, 1995). The bathymetry grid for tsunami numerical simulation has a grid size of 5 arc-min, which was resampled from the General Bathymetric Chart of the Oceans 30 arc-sec dataset. Generally, the numerical model and the grid size are



**Table 1**  
**Seafloor Pressure Sensors Utilized in This Study**

	Instrument Type	Sample Rate (samples/s)	Long-Period Corner (s)
NOAA DART*	Paroscientific absolute pressure gauge <sup>  </sup>	1/15 in event mode	N/A
LDEO APG <sup>†</sup>	Paroscientific absolute pressure gauge <sup>  </sup>	125	N/A
SIO DPG <sup>††</sup>	Cox–Webb differential pressure gauge <sup>#</sup>	50	500
WHOI DPG <sup>§</sup>	Cox–Webb differential pressure gauge <sup>#</sup>	40 (BDH channel) and 1 (LDH channel)	30

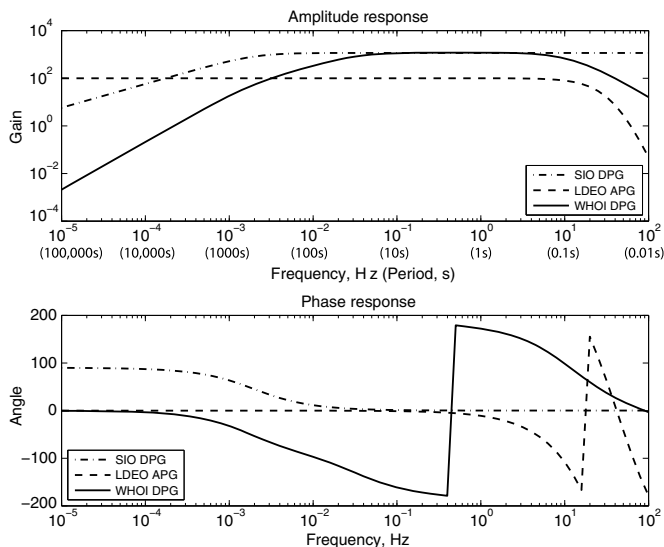
\*National Oceanographic and Atmospheric Administration (NOAA) Deep-ocean Assessment and Reporting of Tsunamis (DART).  
<sup>†</sup>Lamont Doherty Earth Observatory (LDEO) Absolute Pressure Gauge (APG).  
<sup>††</sup>Scripps Institution of Oceanography (SIO) Differential Pressure Gauge (DPG).  
<sup>§</sup>Woods Hole Oceanographic Institution (WHOI) Differential Pressure Gauge (DPG).  
<sup>||</sup>Houston and Paros (1998).  
<sup>#</sup>Cox et al. (1984).

sufficient to accurately simulate tsunami waveforms at offshore locations deeper than 50 m.

We estimated a single-fault model for the 2012 Haida Gwaii earthquake by comparing the observed tsunami waveforms at DART stations with simulated ones adjusted via forward modeling. Seismic *W* phase inversion (Kanamori and Rivera, 2008) is first used to determine earthquake strike 314°, dip 25°, and rake 100°, which we keep fixed in the tsunami modeling. We then adjust fault depth, slip amount, fault length, and fault width to obtain good agreement between observed and simu-

lated tsunami waveforms at the DART stations. Our final model has shallowest part of fault at 1 km, slip amount 2.5 m, fault length 110 km, and fault width 50 km. The location of shallowest northwest corner of the estimated fault model is at 52.1° N, 131.7° W. The calculated seismic moment from the fault model of  $5.5 \times 10^{20}$  N·m ( $M_w$  7.8) is consistent with that from the *W* phase inversion.

The single-fault model can explain the observed amplitude and period of the first cycles of tsunami waveforms at DART stations very well (Fig. 3). However, the single-fault model is too simple to explain the small wiggles in the first cycles of tsunami waveforms. A more complex source model from tsunami waveform inversion may give a slightly better match to the observed tsunami waveforms.



▲ **Figure 2.** Amplitude and phase response of the three different types of seafloor pressure sensors used in the CI, constructed from pole-zero files obtained from Incorporated Research Institutions for Seismology Data Management Center (<http://www.iris.edu/forms/webrequest/>; last accessed March 2015). WHOI differential pressure gauge responses have individually calibrated sensitivity values.

## COMPARISON OF TSUNAMI SYNTHETICS WITH SEAFLOOR PRESSURE OBSERVATIONS

We compare the fit between the observed and simulated tsunami waveforms at the CI pressure sensors to assess the utility of these sensors for tsunami studies. Waveform fits are shown in Figure 3, and show good fits for the first pulse, with a period of  $\sim 1000$  s ( $10^{-3}$  Hz) of the tsunami wave for all instrument types. We observe considerable variation in the waveform amplitude fit by instrument type, and explore that further below. Fits to the DART data are very good in terms of both amplitude and wave period, which is not surprising given that our fault model was determined through modeling of the DART data. Fit to LDEO APG data is very good for the first pulse, including amplitude. Fits after the main pulse, with shorter periods, are not as good, possibly due to near-shore reflected and scattered signals that are not well represented using the coarse bathymetric model. Fits of simulated wavelengths and arrival times to the WHOI DPG data are excellent, though the observed amplitudes are up to a factor of 2 smaller than the simulated amplitudes. The SIO DPGs also fit the main pulse well, and have amplitudes slightly smaller than the synthetics. The SIO DPG data exhibit some long-period artifacts that are

**Table 2**  
**Cascadia Initiative Pressure Sensor Instrument Response**

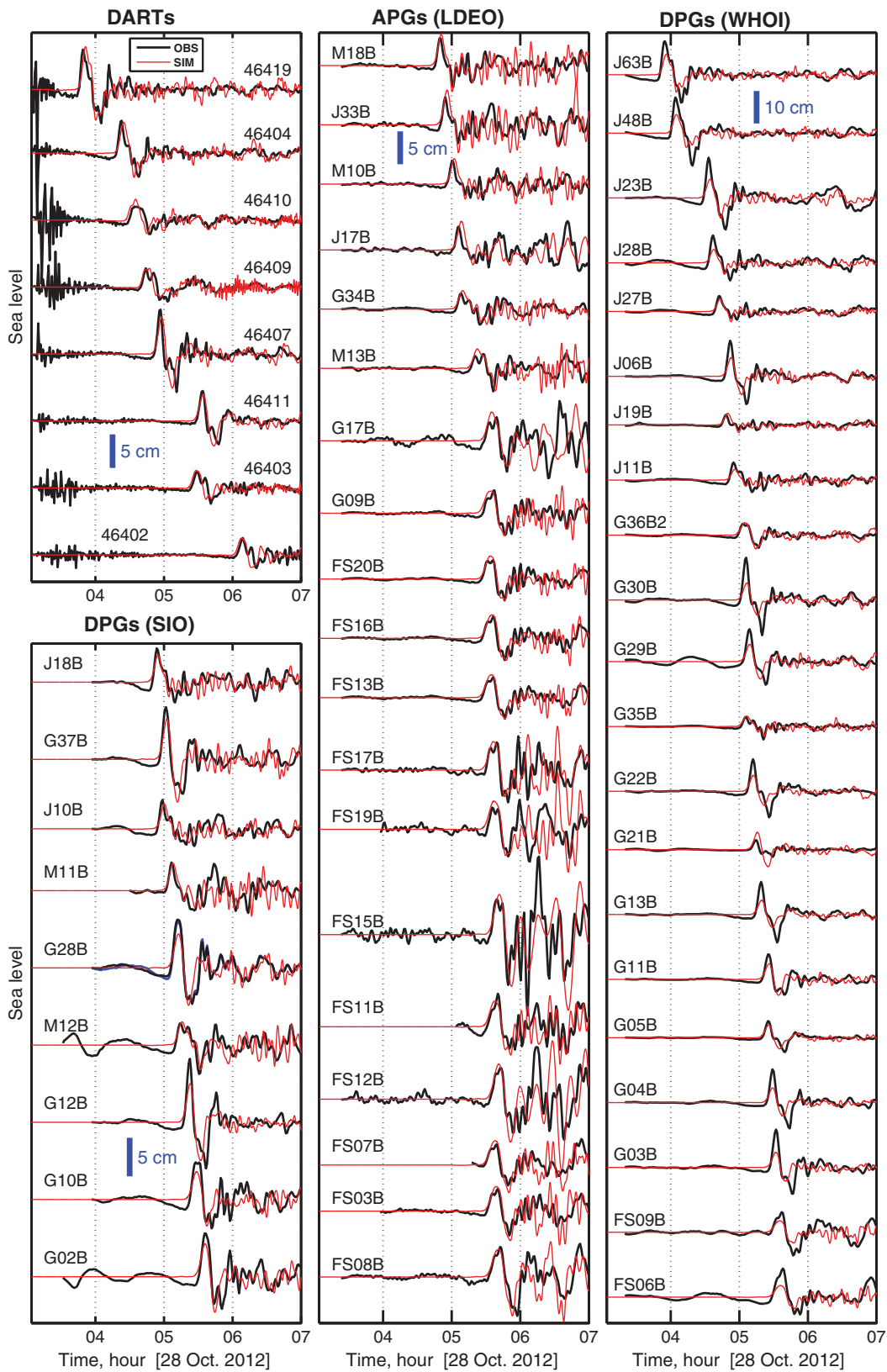
SIO DPG	
Zeros 1	
+0.0000 × 10 <sup>+00</sup>	+0.0000 × 10 <sup>+00</sup>
Poles 1	
-1.2568 × 10 <sup>-02</sup>	+0.0000 × 10 <sup>+00</sup>
Constant	+1.153583 × 10 <sup>+03</sup> (Pa)
WHOI DPG*	
Zeros 3	
+0.0000 × 10 <sup>+00</sup>	+0.0000 × 10 <sup>+00</sup>
+0.0000 × 10 <sup>+00</sup>	+0.0000 × 10 <sup>+00</sup>
-1.1656 × 10 <sup>+04</sup>	+0.0000 × 10 <sup>+00</sup>
Poles 5	
-1.0526 × 10 <sup>-02</sup>	+0.0000 × 10 <sup>+00</sup>
-5.7471 × 10 <sup>+01</sup>	+0.0000 × 10 <sup>+00</sup>
-1.0000 × 10 <sup>+02</sup>	+0.0000 × 10 <sup>+00</sup>
-2.1277 × 10 <sup>-01</sup>	+0.0000 × 10 <sup>+00</sup>
-1.6556 × 10 <sup>+03</sup>	+0.0000 × 10 <sup>+00</sup>
Constant	-9.743110 × 10 <sup>+05</sup> (Pa)
LDEO APG	
Zeros 0	
Poles 8	
-2.6177 × 10 <sup>+02</sup>	+0.0000 × 10 <sup>+00</sup>
-2.6177 × 10 <sup>+02</sup>	+0.0000 × 10 <sup>+00</sup>
-2.6177 × 10 <sup>+02</sup>	+0.0000 × 10 <sup>+00</sup>
-2.6177 × 10 <sup>+02</sup>	+0.0000 × 10 <sup>+00</sup>
-2.6177 × 10 <sup>+02</sup>	+0.0000 × 10 <sup>+00</sup>
-2.6177 × 10 <sup>+02</sup>	+0.0000 × 10 <sup>+00</sup>
-2.6177 × 10 <sup>+02</sup>	+0.0000 × 10 <sup>+00</sup>
-2.6177 × 10 <sup>+02</sup>	+0.0000 × 10 <sup>+00</sup>
Constant	+2.198696 × 10 <sup>+21</sup> (Pa)
Retrieved from IRIS DMC ( <a href="http://www.iris.edu/forms/webrequest/">http://www.iris.edu/forms/webrequest/</a> ; last accessed March 2015).	
*WHOI DPGs are individually calibrated. Constant values vary by approximately 10% with occasional outliers. WHOI KECK and ARRA DPGs have different constants.	

likely due to the instrument deconvolution. The corner period of the SIO DPG is 500 s, and the amplitude response gradually rolls off at longer periods (Fig. 2). Deconvolution amplifies the long-period signals, importantly in the tsunami band of around 1000 s, but also amplifies long-period noise. An additional high-pass filter is applied to the SIO DPG data after deconvolution; however, artifacts remain including long-period signals toward the beginning of the record and a long-period downswing before the main tsunami pulse. Seafloor compliance and dispersion can produce a similar precursory arrival (Watada *et al.*, 2014) but are not thought to play a significant role this close to the source. It is interesting to note that the WHOI DPG data are stable after deconvolution, with no long-period

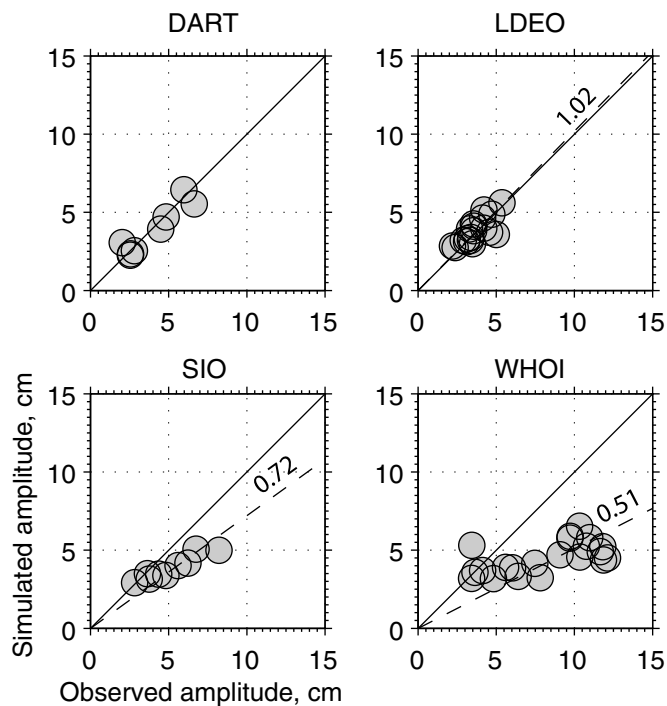
artifacts noted, despite having a higher corner frequency (30 s) than the SIO DPG. A longer period corner and/or more gradual rolloff at long period might improve the SIO DPG tsunami waveform fits, but is hard to justify without further testing.

Peak amplitudes of the main tsunami pulse for both data and the synthetic are compared in Figure 4, with subplots for each instrument type. The dominant period of the first pulse is about 1000 s; hence the comparison may correspond to the amplitude response at around 10<sup>-3</sup> Hz. The match between peak amplitudes of observed and simulated tsunami waveforms at the LDEO APGs is nearly as good as that for the DARTs (Figs. 3 and 4). Some (4 out of 9) of the simulated peak amplitudes at SIO DPGs (J18B, J10B, M11B, and M12B) match the observations very well (Figs. 3 and 4). For the rest of the SIO DPGs, the simulated peak amplitudes are slightly smaller than the observations. Only a few (6 out of 21) of the simulated peak amplitudes at WHOI DPGs (J27B, J19B, J11B, G36B, G35B, and G05B) match the observations very well (Figs. 3 and 4). For the rest of the WHOI DPGs, the simulated peak amplitudes are approximately 2 times smaller than the observations (Fig. 4 lower right panel). We tested whether the peak amplitude fit varies with water depth and found no correlation.

Further comparison between the observed and simulated tsunami waveforms is performed by examination of their coherence in the spectral domain (Fig. 5). The magnitude-squared coherence (called coherence here) is defined as the cross spectrum of two time series divided by the product of the autospectra. Coherence values range from 0 to 1, in which 0 indicates no correlation and 1 indicates maximum correlation between two time series at a given frequency. Coherence between the observed and simulated tsunami waveforms at each station was performed using the MATLAB (<http://www.mathworks.com/help/signal/ref/mscohere.html>; last accessed July 2015) function `mscohere`. In Figure 5, we show two example coherence measurements for each instrument type. The high and flat coherence from about 2 × 10<sup>-4</sup> to 8 × 10<sup>-4</sup> Hz (1250–5000 s) shows that there is good coherence between observations and synthetics for all instrument types in the tsunami band. The coherence measurements further quantify the good fits apparent via visual inspection of the waveforms shown in Figure 3. The oscillations in coherence values at high frequencies are not necessarily significant, and may simply represent that the tsunami synthetics and bathymetry model adopted in this study are more appropriate for long periods than short periods. It is interesting to note that the coherence of the DPG instruments (WHOI and SIO) is comparable to that of the APG instruments (LDEO and DART). In other words, although there are discrepancies between the observed and simulated waves for the DPGs, they match well in terms of wave periods. The coherence of DART data and synthetics is very good, which again is not too surprising because the tsunami source model was chosen to fit the DART data. The WHOI DPGs also perform very well. This might be due in part to the WHOI instruments typically being in deeper water than the LDEO and SIO instruments, though



▲ **Figure 3.** Tsunami waveforms from 28 October 2012 Haida Gwaii earthquake recorded on a subset of DART and CI ocean-bottom pressure recorders. Black curves indicate seafloor pressure records with instrument response removed and converted to water height and red curves indicate simulated waveforms. Waveforms organized by instrument type. Polarity of SIO tsunami waveforms reversed to fit synthetics.

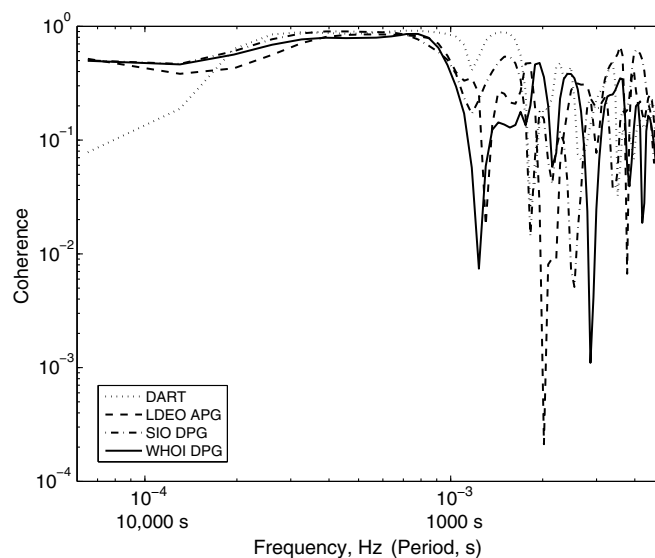


▲ **Figure 4.** Comparison between simulated and observed peak amplitude of tsunami waveforms. Black reference line for slope = 1, best-fit lines (black dashed lines) are given on LDEO, SIO, and WHOI plots. The slopes for the best-fit lines of LEO, SIO, and WHOI are shown on each plot.

this is not always the case. The SIO DPG coherence is not as flat as that for WHOI DPG. That might indicate that there are remaining issues with the SIO instrument response at long periods. The LDEO APG coherence values are high, though perhaps not as flat as expected, given how well the LDEO APGs do with amplitude scaling, but the lack of coherence may have to do with being in shallow water, and further related to an overly smooth bathymetry model.

## DISCUSSION AND CONCLUSIONS

The tsunami signals recorded on both absolute and differential seafloor pressure gauges from the CI experiment are found to be effective for examining tsunami waves. The timing and the waveform shape of the initial tsunami pulse are well fit for all instrument types. The APG instruments perform best in terms of fitting the expected tsunami wave amplitude. The observed DPG amplitudes exhibit scatter ranging from excellent fit to the synthetics to a factor of two low. The scatter suggests that a simple linear scaling to correct the DPG amplitudes would not be sufficient and would result in poorer fits at some stations to improve fits at other stations. The spectral coherence between observed and simulated tsunami waveforms is very good for all instrument types, including both APG and DPG. Our results show, again not particularly surprisingly, that the APG data can be used for tsunami recording including am-



▲ **Figure 5.** Magnitude-squared coherence between observed and simulated tsunami waveforms. Line style denotes instrument type. One sample station for each instrument type shown.

plitude, timing, and waveform spectral character. Our results show that the DPG absolute amplitudes show too much variability for precision amplitude measurements in the tsunami band. The scatter suggests that even relative amplitude studies with the DPG in the tsunami band may be difficult. However, DPG waveform coherence is excellent as well as timing information, suggesting that the DPG data can be used for backprojection, tsunami spectral studies, and other methods that do not require precise amplitudes. The variety of seafloor pressure gauges deployed in the CI experiment provides an excellent opportunity to test the utility of these sensors for a variety of studies, some beyond what the instruments were designed for. The success of recording high-quality tsunami signals on the CI seafloor pressure sensors, both for APGs and DPGs, opens up a new direction of using seafloor pressure data from portable OBS experiments to perform array-based tsunami studies and fill in gaps of DART station coverage. The useful recording of tsunamis on both APG and DPGs demonstrates that temporary OBS networks can be treated as moving arrays of tsunami detectors throughout the world's oceans. ☒

## ACKNOWLEDGMENTS

The authors are grateful to the Cascadia Initiative (CI) Expedition Team for acquiring the Amphibious Array Ocean Bottom Seismograph data and appreciate the open data policy that made the data available shortly after they were acquired. The Scripps, Lamont, and Woods Hole National Ocean Bottom Seismograph Instrument Pool (OBSIP) institutional instrument centers are thanked for building, deploying, and servicing the seafloor instruments of the CI. The facilities of the Incorporated Research Institutions for Seismology (IRIS) Data Management

System were used to access the data used in this study. The IRIS DMS is funded through the United States National Science Foundation under Cooperative Agreement EAR-0552316. We thank Jessica Lodewyk for answering our OBSIP and CI data questions and Justin Ball for help with the coherence measurements. We thank the guest editors of the *SRL* special issue on CI initial results and data quality control, Haiying Gao and Susan Schwartz, and an anonymous reviewer for comments that improved the article. Some of the figures were made using the public domain Generic Mapping Tools (Wessel and Smith, 1998). Partial support for this work came from National Science Foundation Grant Number 1333025 and a University of Colorado College Scholar Award. A. F. S. gratefully acknowledges a visiting professorship at the Earthquake Research Institute, University of Tokyo. M. H. was supported by the Japan Society for the Promotion of Science.

## REFERENCES

- Araki, E., and H. Sugioka (2009). Calibration of deep sea differential pressure gauge, *JAMSTEC-R IFREE* **9**, 141–148.
- Baba, T., K. Hirata, and Y. Kaneda (2004). Tsunami magnitudes determined from ocean-bottom pressure gauge data around Japan, *Geophys. Res. Lett.* **31**, L08303, doi: [10.1029/2003GL019397](https://doi.org/10.1029/2003GL019397).
- Bernard, E. N., F. I. Gonzalez, C. Meinig, and H. B. Milburn (2001). Early detection and real-time reporting of deep-ocean tsunamis, paper presented at the *International Tsunami Symposium 2001 (ITS 2001)*, Seattle, Washington, 7–10 August 2001.
- Chadwick, W. W., S. L. Nooner, D. A. Butterfield, and M. D. Lilley (2012). Seafloor deformation and forecasts of the April 2011 eruption at Axial Seamount, *Nat. Geosci.* **5**, 474–477, doi: [10.1038/NNGEO1464](https://doi.org/10.1038/NNGEO1464).
- Cox, C., T. Deaton, and S. Webb (1984). A deep-sea differential pressure gauge, *J. Atmos. Ocean. Tech.* **1**, 237–346.
- Drushka, K., J. Sprintall, S. T. Gille, and W. S. Pranowo (2008). Observations of the 2004 and 2006 Indian Ocean tsunamis from a pressure gauge array in Indonesia, *J. Geophys. Res.* **113**, no. C07038, doi: [10.1029/2007JC004662](https://doi.org/10.1029/2007JC004662).
- Eble, M. C., and F. González (1991). Deep-ocean bottom pressure measurements in the northeast Pacific, *J. Atmos. Ocean. Tech.* **8**, no. 2, 221–233.
- Fine, I. V., J. Y. Cherniawsky, R. E. Thomson, A. B. Rabinovich, and M. V. Krassovski (2014). *Pure Appl. Geophys.* doi: [10.1007/s00024-014-1012-7](https://doi.org/10.1007/s00024-014-1012-7).
- González, F. I., H. M. Milburn, E. N. Bernard, and J. C. Newman (1998). Deep-ocean Assessment and Reporting of Tsunamis (DART): Brief overview and status report, paper presented at *Proceedings of the International Workshop on Tsunami Disaster Mitigation*, Tokyo, Japan, 19–22 January 1998.
- Houston, M. H., and J. M. Paros (1998). High accuracy pressure instrumentation for underwater applications, *Proc. 1998 Int. Symp. Underwater Technol.*, Tokyo, Japan, 15–17 April 1998, 307–311, doi: [10.1109/UT.1998.670113](https://doi.org/10.1109/UT.1998.670113).
- Ito, Y., T. Tsuji, Y. Osada, M. Kido, D. Inazu, Y. Hayashi, H. Tsushima, R. Hino, and H. Fujimoto (2011). Frontal wedge deformation near the source region of the 2011 Tohoku-Oki earthquake, *Geophys. Res. Lett.* **38**, L00G05, doi: [10.1029/2011GL048355](https://doi.org/10.1029/2011GL048355).
- James, T. S., J. F. Cassidy, G. C. Rogers, and P. J. Haeussler (2015). Introduction to the Special Issue on the 2012 Haida Gwaii and 2013 Craig earthquakes at the Pacific-North America plate boundary (British Columbia and Alaska), *Bull. Seismol. Soc. Am.* **105**, no. 2B, 1053–1057, doi: [10.1785/0120150044](https://doi.org/10.1785/0120150044).
- Kanamori, H., and L. Rivera (2008). Source inversion of *W* phase: Speeding up seismic tsunami warning, *Geophys. J. Int.* **175**, 222–238, doi: [10.1111/j.1365-246X.2008.03887.x](https://doi.org/10.1111/j.1365-246X.2008.03887.x).
- Lay, T., L. Ye, H. Kanamori, Y. Yamazaki, K. F. Cheung, K. Kwong, and K. D. Koper (2013). The October 28, 2012  $M_w$  7.8 Haida Gwaii underthrusting earthquake and tsunami: Slip partitioning along the Queen Charlotte fault transpressional plate boundary, *Earth Planet. Sci. Lett.* **375**, 57–70.
- Leonard, L. J., and J. M. Bednarski (2015). The preservation potential of coastal coseismic and tsunami evidence observed following the 2012  $M_w$  7.8 Haida Gwaii thrust earthquake, *Bull. Seismol. Soc. Am.* **105**, no. 2B, 1280–1289, doi: [10.1785/0120140193](https://doi.org/10.1785/0120140193).
- Lin, F. C., M. D. Kohler, P. Lynett, A. Ayca, and D. S. Weeraratne (2015). The 11 March 2011 Tohoku tsunami wavefront mapping across offshore southern California, *J. Geophys. Res.* **120**, 3350–3362, doi: [10.1002/2014JB011524](https://doi.org/10.1002/2014JB011524).
- Meinig, C., S. E. Stalin, A. I. Nakamura, and H. B. Milburn (2005). Real-time deep-ocean tsunami measuring, monitoring, and reporting system, *The NOAA DART II Description and Disclosure Rep.*, 15 pp.
- Mofjeld, H. O. (2009). Tsunami measurements, in *The Sea: Tsunami*, E. N. Bernard and A. R. Robinson (Editors), Harvard University Press, Cambridge, Massachusetts, 201–235.
- Mungov, G., M. Eblé, and R. Bouchard (2013). DART® Tsunameter retrospective and real-time data: A reflection on 10 years of processing in support of tsunami research and operations, *Pure Appl. Geophys.* **170**, 1369–1384, doi: [10.1007/s00024-012-0477-5](https://doi.org/10.1007/s00024-012-0477-5).
- Polster, A., M. Fabian, and H. Villinger (2009). Effective resolution and drift of Paroscientific pressure sensors derived from long-term seafloor measurements, *Geochem. Geophys. Geosyst.* **10**, Q08008 doi: [10.1029/2009GC002532](https://doi.org/10.1029/2009GC002532).
- Rabinovich, A. B., and M. C. Eble (2015). Deep-ocean measurements of tsunami waves, *Pure Appl. Geophys.* doi: [10.1007/s00024-015-1058-1](https://doi.org/10.1007/s00024-015-1058-1).
- Rabinovich, A., K. Stroker, R. Thomson, and E. Davis (2011). DARTs and CORK in Cascadia basin: High-resolution observations of the 2004 Sumatra tsunami in the northeast Pacific, *Geophys. Res. Lett.* **38**, L08607, doi: [10.1029/2011GL047026](https://doi.org/10.1029/2011GL047026).
- Rawat, A., F. Arduin, V. Ballu, W. Crawford, C. Corela, and J. Aucan (2014). Infragravity waves across the oceans, *Geophys. Res. Lett.* **41**, 7957–7963, doi: [10.1002/2014GL061604](https://doi.org/10.1002/2014GL061604).
- Saito, T., T. Matsuzawa, K. Obara, and T. Baba (2010). Dispersive tsunami of the 2010 Chile earthquake recorded by the high-sampling-rate ocean-bottom pressure gauges, *Geophys. Res. Lett.* **37**, L23303, doi: [10.1029/2010GL045290](https://doi.org/10.1029/2010GL045290).
- Satake, K. (1995). Linear and nonlinear computations of the 1992 Nicaragua earthquake tsunami, *Pure Appl. Geophys.* **144**, 455–470.
- Sheehan, A. F., Z. Yang, D. Nicolsky, G. Mungov, and B. Eakins (2011). Exploring tsunamis with non-traditional dataset: Array recordings from temporary ocean-bottom seismic experiment, *Eos Trans. AGU*, (Fall Meet. Suppl.), Abstract NH33A–1562.
- Takeo, A., D. W. Forsyth, D. S. Weeraratne, and K. Nishida (2014). Estimation of azimuthal anisotropy in the NW Pacific from seismic ambient noise in seafloor records, *Geophys. J. Int.* **199**, 11–22, doi: [10.1093/gji/ggu240](https://doi.org/10.1093/gji/ggu240).
- Thomson, R., I. Fine, A. Rabinovich, S. Mihaly, E. Davis, M. Heesemann, and M. Krassovski (2011). Observation of the 2009 Samoa tsunami by the NEPTUNE-Canada cabled observatory: Test data for an operational regional tsunami forecast model, *Geophys. Res. Lett.* **38**, L11701, doi: [10.1029/2011GL046728](https://doi.org/10.1029/2011GL046728).
- Tian, Y., W. Shen, and M. H. Ritzwoller (2013). Crustal and uppermost mantle shear velocity structure adjacent to the Juan de Fuca Ridge from ambient seismic noise, *Geochem. Geophys. Geosyst.* **14**, 3221–3233, doi: [10.1002/ggge.20206](https://doi.org/10.1002/ggge.20206).

- Titov, V. V., A. Rabinovich, H. O. Mofjeld, R. Thompson, and F. Gonzalez (2005). The global reach of the 26 December 2004 Sumatra tsunami, *Science* **309**, 2045–2048.
- Toomey, D. R., R. M. Allen, A. H. Barclay, S. W. Bell, P. D. Bromirski, R. L. Carlson, X. Chen, J. A. Collins, R. P. Dziak, B. Evers, D. W. Forsyth, P. Gerstoft, E. E. E. Hooft, D. Livelybrooks, J. A. Lodewyk, D. S. Luther, J. J. McGuire, S. Y. Schwartz, M. Tolstoy, A. M. Tréhu, M. Weirathmueller, and W. S. D. Wilcock (2014). The Cascadia initiative: A sea change in seismological studies of subduction zones, *Oceanography* **27**, no. 2, 138–150.
- Watada, S., S. Kusumoto, and K. Satake (2014). Traveltime delay and initial phase reversal of distant tsunamis coupled with the self-gravitating elastic Earth, *J. Geophys. Res.* **119**, 4287–4310, doi: [10.1002/2013JB010841](https://doi.org/10.1002/2013JB010841).
- Webb, S. C., X. Zhang, and W. Crawford (1991). Infragravity waves in the deep ocean, *J. Geophys. Res.* **96**, no. C2, 2723–2736.
- Wessel, P., and W. H. F. Smith (1998). New, improved version of generic mapping tools released, *Eos Trans. AGU* **79**, 579, doi: [10.1029/98EO00426](https://doi.org/10.1029/98EO00426).

*Anne F. Sheehan*  
*Department of Geological Sciences and Cooperative Institute*  
*for Research in Environmental Sciences*  
*UCB 399, University of Colorado*  
*Boulder, Colorado 80309 U.S.A.*  
*anne.sheehan@colorado.edu*

*Aditya Riadi Gusman*  
*Mohammad Heidarzadeh*  
*Kenji Satake*  
*Earthquake Research Institute*  
*University of Tokyo*  
*1-1-1 Yayoi, Bunkyo-ku*  
*Tokyo 113-0032, Japan*

Published Online 19 August 2015